Signatures of self-modulation effects during pulse propagation in single-pulse absorption spectra

Yu He,[1] Zuoye Liu,[1,*] Zuwen Cui,[1] Yuxuan Zhang,[1] Adrian N. Pfeiffer,[2] Thomas Pfeifer,[3] Jingjie Ding,[1,†] and Bitao Hu[1]

[1]*School of Nuclear Science and Technology, Lanzhou University, 730000 Lanzhou, China*

[2]*Institute of Optics and Quantum Electronics, Friedrich Schiller University, Max-Wien-Platz 1, 07743 Jena, Germany*

[3]*Max-Planck-Institut für Kernphysik, Saupfercheckweg 1, 69117 Heidelberg, Germany*

(Received 12 February 2019; revised manuscript received 1 April 2019; published 20 May 2019)

The absorption spectrum of a bound state with a finite lifetime gives rise to the well-known Lorentzian line shape. This fundamental mechanism breaks down at high intensities. Here we demonstrate how even a single intense multicycle excitation pulse can result in Fano absorption profiles in the frequency domain. The intensity-dependent line shapes indicate the dipole responses are phase modulated by the single excitation pulse itself. Further, as the atomic density increases, we observe broader Fano-like shapes and the appearance of novel substructures in absorption lines. These are clear signatures of propagation effects in which collective interactions need to be taken into account. An analytical model is applied, which describes both effects observed in the experiment. Understanding the transition from optically dilute to dense medium is crucial to distinguish between single-atom and macroscopic effects.

DOI: 10.1103/PhysRevA.99.053418

I. INTRODUCTION

Spectral line shapes encode structural and dynamical properties of quantum systems, specifically, their optical dipole responses. Most commonly, symmetric Lorentzian absorption lines are obtained from excited bound states, while asymmetric Fano profiles are caused by discrete states coupled to a continuum [1]. Recently a laser-control mechanism was demonstrated [2], in which the presence of a time-delayed pulse after excitation can modify natural Fano profiles to Lorentzian ones and vice versa via transient energy shifts, e.g., ac Stark shifts or ponderomotive energy shifts. Quantities of theoretical and experimental studies [2–5] have tried to pinpoint the link between the spectral line shape and the phase shift of the time-domain dipole. The phase extracted from the absorption spectrum carries dynamical information, enabling the direct reconstruction of wave-packet dynamics [6–8], and *in situ* characterization of laser pulses [9]. Besides, causality even unlocks the possibility to temporally resolve the response of a system from a single spectrum [10]. The temporal evolution of spectral lines has been reported to provide direct access to real-time quantum dynamics by transient absorption spectroscopy [11–14].

However, the vast majority of transient absorption experiments assume the prior excitation pulse is short and weak. But some other investigations have shown that the finite-duration and high-intensity-nature of a pulse play a role, for instance, population inversion in air lasing induced by postionization couplings [15,16]. More severely, even though the optical densities are relatively large among some of these experiments, the dilute gas assumption is employed by default. For dilute gases, the measured optical density (OD) is directly proportional to the single-atom absorption cross section and thus to the imaginary part of dipole response function in the frequency domain:

$$\mathrm{OD}(\omega) \propto \mathrm{Im}[d(\omega)], \tag{1}$$

with $d(\omega)$ being connected to the temporal response $d(t)$ via Fourier transform. Modifications after propagation through the medium are ignored. So far only few attempts [17–24] have addressed the roles of macroscopic effects in photoabsorption beyond Beer-Lambert law, and the transition of laser-modified line shapes from the dilute-gas limit to the high still remains mysterious.

Here, we observe and model the breakdown of two key approximations: the weak-excitation and the dilute-gas limits. The general model is able to describe the entire transition from the limiting cases where the approximation holds into the deep intensity- and density-dominated regime. In our experiments, we employ atomic Rb vapor in a static absorption cell, allowing control of the atomic density by the cell temperature. We explore the spectral line-shape evolutions for different temperatures and pulse intensities. The observations are identified as the combined contribution of self-modulation and propagation effects. Since laser spectroscopy aims to capture and resolve dynamical processes on ultrafast timescales, understanding these fundamental phenomena in absorption spectra caused by a single pulse alone lays the foundation towards transient absorption spectroscopy in the presence of intense pump or probe pulses. More generally, incorporating such effects is also indispensable to the investigations of complex systems such as large molecules [25] and solids [26,27].

II. EXPERIMENTAL METHOD

A schematic illustration of the experimental setup is depicted in Fig. 1(a). Our experiment utilizes a commercial Ti:sapphire chirped-pulse amplification laser system to deliver transform-limited pulses at a repetition rate of 1 kHz with

*Corresponding author: zyl@lzu.edu.cn

†Corresponding author: dingjj@lzu.edu.cn

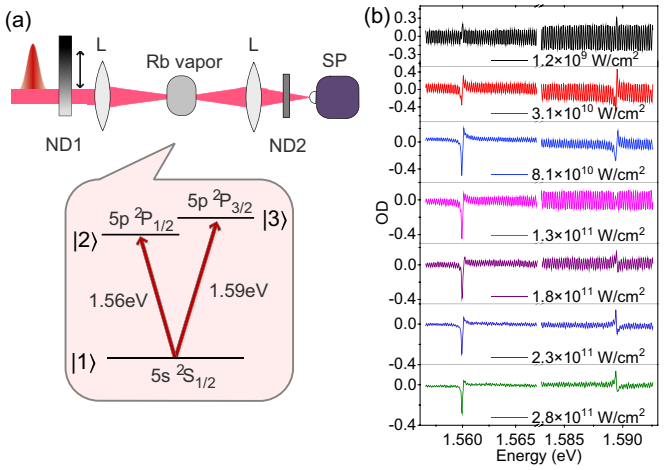

FIG. 1. (a) Schematic of the experimental setup for single-pulse absorption spectroscopy. L, focusing lens; SP, spectrometer; ND1 and ND2, neutral density filters. The inset shows the relevant energy-level diagram. (b) Experimentally measured absorption line-shape evolution as a function of pulse intensity at 70 °C, in the dilute gas limit.

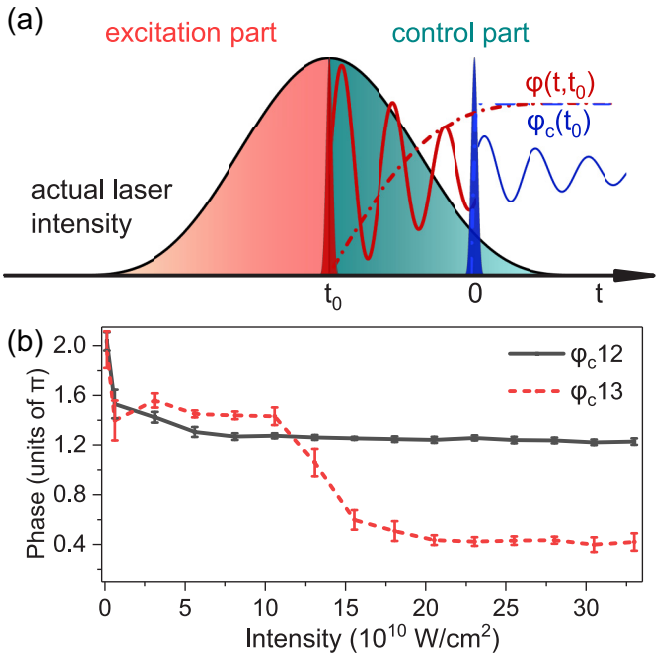

FIG. 2. (a) Analytical model. The actual laser is divided into excitation part (red shaded area) and control part (green shaded area) artificially. The dipole response excited at the peak of the pulse envelope is phase modulated by the following control part. Instead of an accumulative intensity-dependent phase $\varphi(t, t_0)$ (red dash-dotted line), this self-modulation effect is approximated by an instantaneous phase jump $\varphi_c(t_0)$ at $t = 0$ (blue dashed line). (b) Phases extracted from measured spectra as a function of pulse intensity. Error bars depict the standard error of the values in the fitting procedure.

pulse duration of 30 fs and central wavelength of 800 nm. Rb vapor is held in a cell with effective length of 22 mm and two 1.5-mm-thick BK7-glass windows on both ends. In the measurement, the temperature is varied from 70–160 °C by a homemade heating and control system, and the atomic densities are estimated by their corresponding vapor pressures [28]. For these temperatures, the atomic density is estimated to range from 7.4×10^{11} to 1.6×10^{14} cm^{-3}. A continuously variable density filter (ND1) is inserted in the beam path to tune the laser intensity, and the maximum pulse intensity applied is around 3×10^{11} W/cm^2, limited by laser filamentation in the front window. The measured absorption spectrum is characterized by the optical density, $\mathrm{OD}(\omega) = \ln[I_0(\omega)/I(\omega)]$, where $I_0(\omega)$ and $I(\omega)$ are the incoming and transmitted spectra resolved by a fiber-pigtailed spectrometer (McPherson 2061). The spectral range is set just to cover the two single-electron transitions $5s\ ^2S_{1/2} \rightarrow 5p\ ^2P_{1/2}$ ($|1\rangle \rightarrow |2\rangle$ at 794.76 nm) and $5s\ ^2S_{1/2} \rightarrow 5p\ ^2P_{3/2}$ ($|1\rangle \rightarrow |3\rangle$ at 780.03 nm) with a resolution of ≈0.035 meV. Lifetimes of the upper states are in the nanosecond range [29], much shorter than the time interval between two consecutive pulses. Even if the dephasing times are shorter than the lifetimes, they are still orders of magnitude longer than the femtosecond pulses. These considerations are essential in our latter discussions.

III. SELF-MODULATION EFFECTS

The intensity-dependent line-shape modification is first investigated within the single-atom response by heating the cell to 70 °C, corresponding to a relatively low atomic density. Figure 1(b) shows the measured OD spectra around the transition frequencies for different pulse intensities. It should be noted that within the approximation of weak excitation, the exponentially decaying dipoles result in natural Lorentzian absorption line shapes in the absence of an external field. However, the condition breaks down as we observe the lines no longer stay Lorentzian. Instead, asymmetric Fano profiles emerge for increasing intensity, implying the dipole responses of the system are phase modulated. Since the time interval between two consecutive pulses is 1 ms, this intensity-dependent observation must be attributed to the excitation pulse itself. Actually, the whole part of the electric field contributes to the excitation. For a straightforward interpretation of the phenomenon and to include the self-modulation effects for simplicity, we divide the laser pulse into excitation and control parts as shown in Fig. 2(a). In this way, an intuitive physical picture is presented. We model the polarization response to be initialized at the peak of laser pulse envelope, and the subsequent control part to Stark shift the excited states. It thus imprints an additional phase $\varphi(t, t_0) = \int_{T_c} \Delta E(t, t_0) dt$, where ΔE represents the transient energy shift of the upper level. Now that the interaction period T_c is shorter than the pulse duration and is negligible compared to the dephasing time of both states, this manipulation can be treated as an instantaneous phase step at $t = 0$. Hence the disturbed dipole response function is described as (atomic units are used unless otherwise noted)

$$d(t, t_0) \propto \begin{cases} 0 & t < t_0 \\ ie^{(-i\omega_0 - \Gamma/2)(t - t_0)} & t_0 \leqslant t < 0. \\ ie^{(-i\omega_0 - \Gamma/2)(t - t_0)} e^{i\varphi_c(t_0)} & 0 \leqslant t \end{cases} \quad (2)$$

Here, ω_0 denotes the transition frequency and Γ the decay rate. To efficiently account for Doppler broadening and

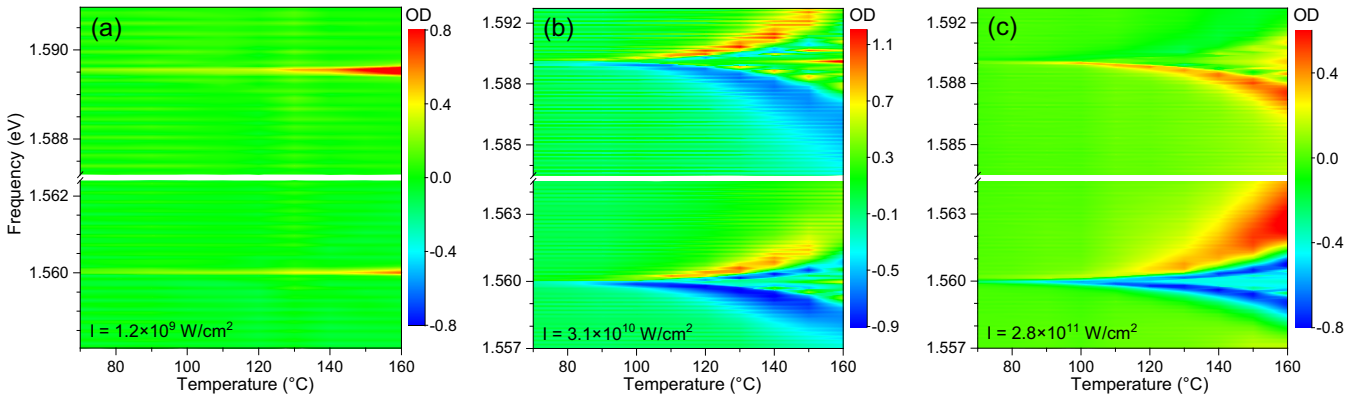

FIG. 3. Experimental absorption spectrum as a function of temperature with a fixed pulse intensity (a) $I = 1.2 \times 10^9$ W/cm^2, (b) $I = 3.1 \times 10^{10}$ W/cm^2, and (c) $I = 2.8 \times 10^{11}$ W/cm^2. As the temperature rises, line profiles around the two transitions broaden slightly but remain symmetric in (a). While in (b) and (c), other than the bigger broadening, complicated spectral subfeatures arise at a relatively high temperature.

collision-induced broadening in the measurement, we use $\Gamma_{12} = \Gamma_{13} = 1/(7\ \text{ps})$ to approximate the experimental line widths. $t_0 = -30$ fs is applied for the present case, and a slight change of this value was confirmed not to alter the results much. The system evolves freely before the self-induced phase shift is added at $t = 0$. Afterwards, the temporal structure is again governed by field-free evolution. Fitting the measured spectra with Eq. (1) and Fourier transform (centered at $t = t_0$) of Eq. (2), we extract the phases $\varphi_c 12$ and $\varphi_c 13$ as shown in Fig. 2(b). With the relation between OD(ω) and φ_c, the fitting procedure was implemented with a standard algorithm, *Mathematica*'s FINDFIT with the method NMINIMIZE, which gave a globally best fit and the standard error. Only the data around the resonance frequencies were involved, since they greatly outweigh the nonresonant components. These artificial phases reflect the interaction strength. The modulation effect typically increases with a stronger laser pulse, showing as approximately monotonous decrease for both resonances. A more remarkable intensity dependence is displayed for $\varphi_c 13$, as the stronger $|1\rangle \rightarrow |3\rangle$ transition is more susceptible to external light fields. However, complex higher-order (e.g., Raman) processes between the resonances and further excitation and/or ionization of Rb can lead to deviations from the simple monotonous behavior. The near-constant plateaus suggest the electronic dipoles become more and more insensitive to the laser pulse with the increase of pulse intensity. A rigorous explanation of this behavior demands for more advanced numerical calculations, including more atomic levels, and possibly ionization.

IV. PROPAGATION EFFECTS

To explore the dependence on gas density, in the following the cell temperature is varied. Figure 3 shows the results measured with different laser intensities. At low pulse energy where self-modulation effects are negligible, the natural Lorentzian lines broaden slightly and their shapes remain symmetric [see Fig. 3(a)]. While in Figs. 3(b) and 3(c), the spectra exhibit complicated features with substructures emerging and dominating. Corresponding line-shape evolutions are shown in Figs. 4(a) and 4(c). As the temperature rises, the overall absorption profiles broaden initially, with characteristic absorption peaks and emission valleys both moving outward from the center of lines, while approximately maintaining their shapes. This implies that the self-induced phases are temperature-independent. Subsequently, several

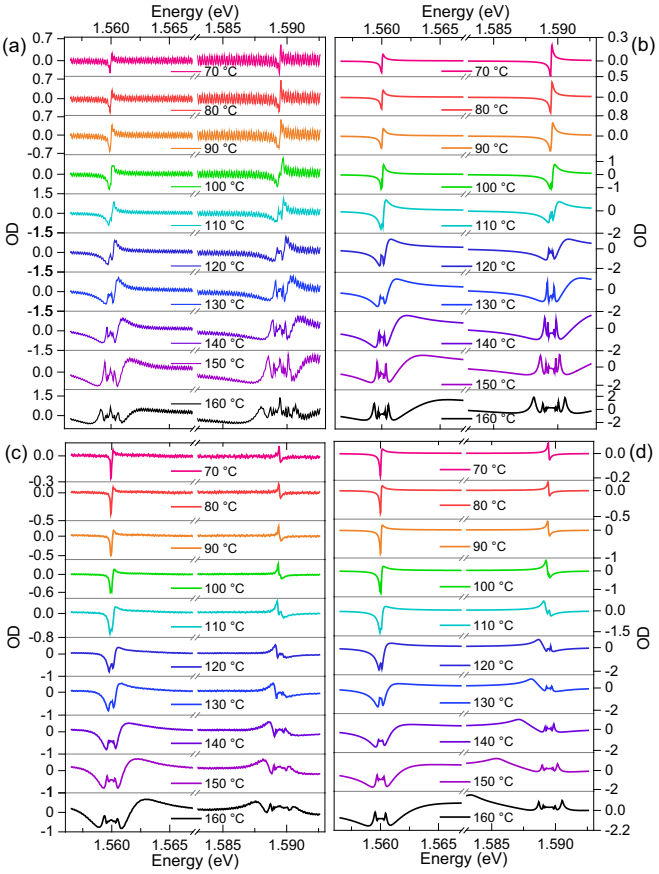

FIG. 4. (a), (c) Experimental and (b), (d) theoretical spectral line shapes at fixed pulse intensities [3.1×10^{10} W/cm^2 in (a) and (b), 2.8×10^{11} W/cm^2 in (c) and (d)] with varying temperature. The characteristic Fano profiles are heavily distorted at sufficiently high cell temperatures.

substructures emerge close to the line center and move outward. Further rise of temperature even splits and enhances the substructures such that they become comparable to or stronger than the original Fano peaks, making the entire spectral lines too complex to characterize intuitively.

The atomic density inside the cell increases with the temperature, resulting in a greater optical thickness. This density-dependent line-shape modification closely resembles observations in several recent attosecond transient absorption experiments [23,24], pointing towards similar underlying mechanisms. The calculation of propagation effects in laser-controlled media can in principle be solved by numerically integrating the coupled time-dependent Schrödinger equation (TDSE) and the Maxwell wave equation (MWE) [23,24]. However, for long-lived states with decay times longer than picoseconds, the approach of a time-domain integration is unfeasible due to exceedingly large computation times. Accordingly, a frequency-domain approach is required.

A suited approach has been presented recently by Pfeiffer *et al.* [22]. It is an extension of the model that we used in the previous section, but it goes beyond the single-atom response. It was derived from the Liouville-von Neumann equation and takes consideration of macroscopic effects. The core is the following analytical formula for the polarization response:

$$d(\omega, x, t_0) = \chi(\omega) E_e(\omega, x, t_0) + i\chi(\omega)\frac{(L-1)Q(x, t_0)}{\sqrt{8\pi}N\mu^2}. \quad (3)$$

This analytic formula is expressed in the frequency domain, circumventing the need for a time integration. In the original publication [22], t_0 (δt) referred to the pulse delay in a transient absorption experiment. Here, we use the formula with the assumption that t_0 refers to the effective time when the laser-induced phase shift occurs, just like in the previous paragraphs. Equation (3) includes macroscopic propagation effects, and N denotes the atomic number density and x is the coordinate of propagation (χ, L, and Q are defined further below). The equation requires the knowledge of the electric field of the excitation pulse at position x, represented by E_e, which undergoes deformations as the pulse travels along x. Therefore, the numerical integration in the direction of laser propagation still needs to be performed, but the computational effort is rather low. Here, we use the following approximated wave equation [18]

$$\frac{\partial}{\partial x} E_e(\omega, x, t_0) = -2\pi i \frac{\omega}{c} d(\omega, x, t_0) \quad (4)$$

for the spatial integration. After the numerical integration, the space-dependent absorbance is readily calculated as

$$\mathrm{OD}(\omega, x, t_0) = \ln\left[\frac{|E_e(\omega, 0, t_0)|^2}{|E_e(\omega, x, t_0)|^2}\right]. \quad (5)$$

At low pulse energy, the polarization response is linear and the first part of Eq. (3) is sufficient. The linear response is calculated using the susceptibility $\chi(\omega)$, which is approximated by

$$\chi(\omega) = \frac{2N\omega_0\mu^2}{{\omega_0}^2 - \omega^2 + i\Gamma\omega}. \quad (6)$$

The analytic solution of Eq. (4), when only the linear response of Eq. (3) is used, reproduces the Beer-Lambert law. At higher pulse energy, an additional modification is introduced, which is expressed in the second part of Eq. (3). L is the polarization modification and is treated as pure phase changes $L = e^{-i\varphi_c(t_0)}$ with $\varphi_c(t_0)$ extracted at 70 °C (i.e., low OD) described above. To apply the phase shift, an expression for the field at instance t_0 at propagation distance x is required, which is expressed by the parameter $Q(x, t_0)$ [22].

$$Q(x, t_0) = \frac{2}{\sqrt{2\pi}} \int_0^\infty \chi(\omega) E_e(\omega, 0, t_0) e^{-2\pi i \frac{\omega}{c}\chi(\omega)x} d\omega \quad (7)$$

describes the complex valued polarization response at the time of the laser-induced phase shift L. A parameter $p_1(\omega) = |\chi(\omega)|\omega x/c$ has been deduced as a criterion to assess the severity of macroscopic effects [22], which is a measure of the absolute value of the accumulated spectral phase. Propagation effects are of importance when p_1 is on the order of 1 and can be neglected for $p_1 \ll 1$. For the present case, $p_1(\omega_{12})$ and $p_1(\omega_{13})$ reach this critical value at the temperature of ≈120 °C. This can also be verified from Figs. 3(b) and 3(c), as the absorption lines begin to change substantially at around 120 °C.

To understand that the macroscopic propagation leads to rich spectral features, it is illustrative to discuss the evolution of the field waveform during propagation. Crisp [30] and Lamb [31] have first discussed this temporal evolution of a short pulse propagating through a medium for the case of linear response. During transmission, the pulse envelope undergoes reshaping and develops a tail, which decays with a decay time determined by the inverse of the absorption line width. In consecutive propagation, shorter and shorter subpulses are formed within the tail, and the electric field in each subpulse changes its phase by π relative to the previous one. Initially, the electric field in the tail (generated by the resonantly excited time-dependent dipole moment) is π phase shifted with respect to the driving field, which causes destructive interference and gives rise to a spectral hole at transition energies, i.e., Lorentzian absorption lines. In consecutive propagation steps, however, the addition of phase shifts alters the dipole responses, and the newly generated fields will not be exactly π out of phase with the driving field any more. When a laser-induced phase factor L is introduced by nonlinear interaction, then intricate spectral features arise. With increasing optical thickness, the dispersive absorption line shape does not evolve linearly but yields more complicated characteristics.

In our calculation, the two transitions are solved independently, and the atomic number density and decay rates are slightly adjusted to match the experimentally observed line shapes. Simulation results in Figs. 4(b) and 4(d) illustrate the roles of density-dependent propagation effects. Note that only electric-dipole-allowed transitions are considered for the present pulse intensities, we use dipole moments $\mu_{12} = 1.75$, $\mu_{13} = \sqrt{2}\mu_{12} = 2.47$ [32]. The stronger single-atom response around ω_{13} renders a more notable spectral reshaping as shown in Fig. 4. Generally, propagation through the resonant medium leads an energy redistribution between the light field and the atomic system in multiple scattering and generates renewed absorption profiles. Apart from the bigger broadening, essential features are basically captured in the analytical approximation. Deviations may originate from

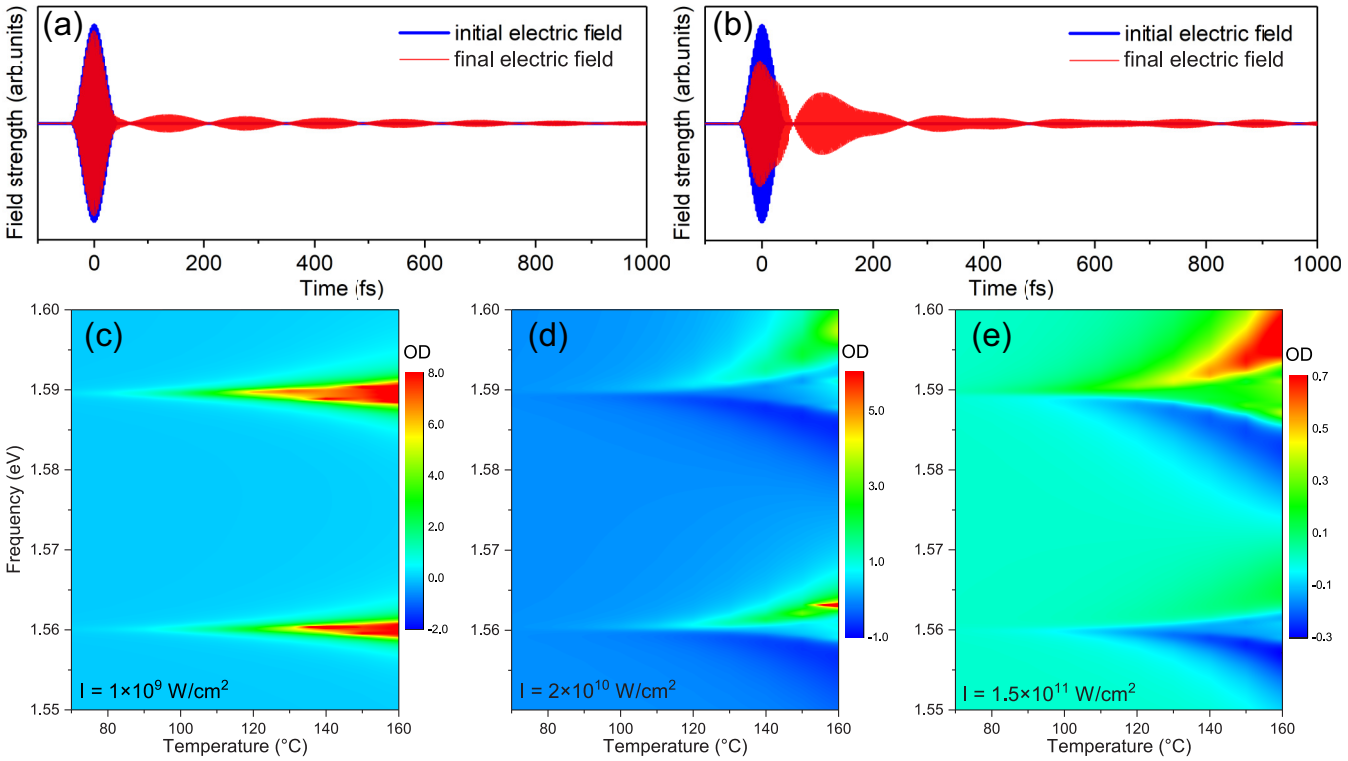

FIG. 5. Numerical calculations. Time-domain illustration of initial and final electric field with a pulse intensity $I = 1 \times 10^9$ W/cm^2 at (a) 120 °C and (b) 160 °C. Theoretical absorption spectrum versus cell temperature with a fixed pulse intensity (c) $I = 1 \times 10^9$ W/cm^2, (d) $I = 2 \times 10^{10}$ W/cm^2, and (e) $I = 1.5 \times 10^{11}$ W/cm^2. Spectral evolutions are similar with the observed results in Figs. 3(a)–3(c).

the propagation-controlled lifetime becoming comparable to the timescale of phase modulation, by which the final line shape turns out to be narrower than propagation effects would predict, as discussed in Ref. [23].

It is interesting to note that our treatment of macroscopic propagation is consistent with the previous treatment of dilute samples. Specially, for the limiting case of a thin medium ($x = 0$), Eq. (3) reduces to

$$d(\omega, 0, t_0) = \chi(\omega) E_e(\omega, 0, t_0)[1 + (L-1)e^{[i(\omega-\omega_0)+\Gamma/2]t_0}]. \tag{8}$$

The equation is equivalent to Eq. (2), except for the conjugated expression in polarization modification.

V. NUMERICAL RESULTS

In the following, numerical calculations are performed with a three-level model to support our above results. The theoretical framework is described in terms of density matrix form with the inclusion of macroscopic effects. The atomic system is approximated by a 3×3 density matrix $\hat{\rho}(t)$, and its dynamical evolution results from the Liouville-von Neumann equation

$$i\frac{\partial \hat{\rho}(t)}{\partial t} = [\hat{H}(t), \hat{\rho}(t)] - i\hat{\gamma} \circ \hat{\rho}(t). \tag{9}$$

The Hamiltonian $\hat{H}$ in the dipole approximation is defined as $\hat{H}(t) = \hat{H}_0 - \hat{\mathbf{M}}E(t)$, where $\hat{H}_0$ is the electronic-structure Hamiltonian and $\hat{\mathbf{M}}$ the dipole matrix. $\hat{\gamma}$ is a phenomenological decay matrix, which includes both decay of the state populations and the coherences. We use $\gamma_{22} = \gamma_{33} = 1/(600$ fs) in the calculation for the feasibility of the computation. The polarization response $d(t)$ is given by

$$d(t) = N\mathrm{Tr}[\hat{\rho}(t)\hat{\mathbf{M}}]. \tag{10}$$

To go beyond the single-atom response, the spatial evolution of light field along x is considered and approximated by the wave equation (4). At each spatial point, we solve the Liouville equation (9) by direct integration to evaluate the polarization response through Eq. (10). Then, we insert the Fourier transform of it into the Eq. (4) to step forward. The absorbance after a propagation length x can thus be obtained by Eq. (5). In our calculation, the atomic densities are multiplied by 3 to mimic the experimental results.

Figure 5 shows the numerical results in the consideration of propagation effects. In Figs. 5(a) and 5(b), the electric field develops a long tail consisting of a series of lobes after propagation through the medium. Stronger subpulses are formed with a larger atomic density, and each subpulse in the tail is weaker than the former one. Figures 5(c)–5(e) show the theoretical absorption spectra using comparable pulse intensities with respect to Figs. 3(a)–3(c). Although there are visible deviations between them, the calculated spectral features are quite close to the experimental observations. The analytical solution described in the previous sections relies on extracting the phase information from measured spectrum. The recovered phases enable us to analyze the modulation effects and reproduce the absorption line shapes. By contrast, the numerical calculations performed here are limited to the approximation of a three-level system. Further excitation to

higher $5d\ ^2D_{3/2,5/2}$ states (which are also resonantly excited by the optical pulse, albeit more weakly than the $|1\rangle \rightarrow |2\rangle, |3\rangle$ transitions), as well as photoionization can lead to the deviations. However, these factors are beyond the current considerations.

VI. CONCLUSIONS

In summary, we employ single-pulse absorption spectroscopy to observe and understand the breakdown of the weak-field and low-density approximations. A general model is applied, which suffices to describe the observations from the limit where the single-atom response approximation holds, to the optically dense cases in which propagation effects play a crucial role in line-shape control. The resulting spectral lines are governed by the coexistence of self-modulation and propagation effects. The phase information encoded in the absorption spectrum seems not straightforwardly extractable when propagation effects are entangled, particularly in dense media. Parameter p_1 gives an estimation of the severity of propagation effects, and the case when p_1 is larger than or on the order of 1 deserves more attention. Reconstruction of quantum dynamics demands separation of single-atom versus propagation effects, which reflect differently in the experimentally observed line shapes. The good agreement between theoretical results and measurements here also allows us to shape light fields by the combined action of intense-field and propagation effects, consequently paving the way towards controlling quantum processes on ultrafast timescales.

ACKNOWLEDGMENTS

The authors thank National Natural Science Foundation of China (Grants No. 11504148 and No. 11575073) and the Fundamental Research Funds for the Central Universities (Grant No. lzujbky-2016-35).

[1] U. Fano, Phys. Rev. **124**, 1866 (1961).
[2] C. Ott, A. Kaldun, P. Raith, K. Meyer, M. Laux, J. Evers, C. H. Keitel, C. H. Greene, and T. Pfeifer, Science **340**, 716 (2013).
[3] S. Pabst, A. Sytcheva, A. Moulet, A. Wirth, E. Goulielmakis, and R. Santra, Phys. Rev. A **86**, 063411 (2012).
[4] A. Kaldun, C. Ott, A. Blättermann, M. Laux, K. Meyer, T. Ding, A. Fischer, and T. Pfeifer, Phys. Rev. Lett. **112**, 103001 (2014).
[5] H. Mashiko, T. Yamaguchi, K. Oguri, A. Suda, and H. Gotoh, Nature Commun. **5**, 5599 (2014).
[6] A. Blättermann, C. Ott, A. Kaldun, T. Ding, and T. Pfeifer, J. Phys. B: At., Mol. Opt. Phys. **47**, 124008 (2014).
[7] C. Ott, A. Kaldun, L. Argenti, P. Raith, K. Meyer, M. Laux, Y. Zhang, A. Blättermann, S. Hagstotz, T. Ding *et al.*, Nature (London) **516**, 374 (2014).
[8] Z. Liu, S. M. Cavaletto, C. Ott, K. Meyer, Y. Mi, Z. Harman, C. H. Keitel, and T. Pfeifer, Phys. Rev. Lett. **115**, 033003 (2015).
[9] A. Blättermann, C. Ott, A. Kaldun, T. Ding, V. Stooß, M. Laux, M. Rebholz, and T. Pfeifer, Opt. Lett. **40**, 3464 (2015).
[10] V. Stooß, S. M. Cavaletto, S. Donsa, A. Blättermann, P. Birk, C. H. Keitel, I. Březinová, J. Burgdörfer, C. Ott, and T. Pfeifer, Phys. Rev. Lett. **121**, 173005 (2018).
[11] E. Goulielmakis, Z.-H. Loh, A. Wirth, R. Santra, N. Rohringer, V. S. Yakovlev, S. Zherebtsov, T. Pfeifer, A. M. Azzeer, M. F. Kling *et al.*, Nature (London) **466**, 739 (2010).
[12] S. R. Leone, C. W. McCurdy, J. Burgdörfer, L. S. Cederbaum, Z. Chang, N. Dudovich, J. Feist, C. H. Greene, M. Ivanov, R. Kienberger, U. Keller, M. F. Kling, Z.-H. Loh, T. Pfeifer, A. N. Pfeiffer, R. Santra, K. Schafer, A. Stolow, U. Thumm, and M. J. J. Vrakking, Nature Photonics **8**, 162 (2014).
[13] K. Ramasesha, S. R. Leone, and D. M. Neumark, Annu. Rev. Phys. Chem. **67**, 41 (2016).
[14] M. Sabbar, H. Timmers, Y.-J. Chen, A. K. Pymer, Z.-H. Loh, S. G. Sayres, S. Pabst, R. Santra, and S. R. Leone, Nature Phys. **13**, 472 (2017).
[15] H. Xu, E. Lötstedt, A. Iwasaki, and K. Yamanouchi, Nature Commun. **6**, 8347 (2015).
[16] J. Yao, S. Jiang, W. Chu, B. Zeng, C. Wu, R. Lu, Z. Li, H. Xie, G. Li, C. Yu, Z. Wang, H. Jiang, Q. Gong, and Y. Cheng, Phys. Rev. Lett. **116**, 143007 (2016).
[17] M. B. Gaarde, C. Buth, J. L. Tate, and K. J. Schafer, Phys. Rev. A **83**, 013419 (2011).
[18] R. Santra, V. S. Yakovlev, T. Pfeifer, and Z.-H. Loh, Phys. Rev. A **83**, 033405 (2011).
[19] W.-C. Chu and C. D. Lin, Phys. Rev. A **87**, 013415 (2013).
[20] C. D. Lin and W.-C. Chu, Science **340**, 694 (2013).
[21] S. Chen, M. Wu, M. B. Gaarde, and K. J. Schafer, Phys. Rev. A **88**, 033409 (2013).
[22] A. N. Pfeiffer, M. J. Bell, A. R. Beck, H. Mashiko, D. M. Neumark, and S. R. Leone, Phys. Rev. A **88**, 051402(R) (2013).
[23] C.-T. Liao, A. Sandhu, S. Camp, K. J. Schafer, and M. B. Gaarde, Phys. Rev. Lett. **114**, 143002 (2015).
[24] C.-T. Liao, A. Sandhu, S. Camp, K. J. Schafer, and M. B. Gaarde, Phys. Rev. A **93**, 033405 (2016).
[25] K. Meyer, Z. Liu, N. Müller, J.-M. Mewes, A. Dreuw, T. Buckup, M. Motzkus, and T. Pfeifer, Proc. Natl. Acad. Sci. USA **112**, 15613 (2015).
[26] M. Schultze, K. Ramasesha, C. Pemmaraju, S. Sato, D. Whitmore, A. Gandman, J. S. Prell, L. J. Borja, D. Prendergast, K. Yabana, D. M. Neumark, and S. R. Leone, Science **346**, 1348 (2014).
[27] M. Lucchini, S. A. Sato, A. Ludwig, J. Herrmann, M. Volkov, L. Kasmi, Y. Shinohara, K. Yabana, L. Gallmann, and U. Keller, Science **353**, 916 (2016).
[28] D. A. Steck, Rubidium 85 d line data, revision 2.1.6, 2013, https://steck.us/alkalidata/.
[29] C. E. Theodosiou, Phys. Rev. A **30**, 2881 (1984).
[30] M. D. Crisp, Phys. Rev. A **1**, 1604 (1970).
[31] G. L. Lamb, Rev. Mod. Phys. **43**, 99 (1971).
[32] R. Netz, T. Feurer, G. Roberts, and R. Sauerbrey, Phys. Rev. A **65**, 043406 (2002).